Title
Preindustrial atmospheric ethane levels inferred from polar ice cores: A constraint on the geologic sources of atmospheric ethane and methane

Journal
Geophysical Research Letters, 43(1)

ISSN
0094-8276

Authors
Nicewonger, Melinda R
Verhulst, Kristal R
Aydin, Murat
et al.

Publication Date
2016-01-16

DOI
10.1002/2015gl066854

AGU PUBLICATIONS

Geophysical Research Letters

RESEARCH LETTER
10.1002/2015GL066854

Key Points:
- First measurements of ethane in polar ice cores
- Preindustrial atmospheric ethane levels significantly lower than today
- Geologic emissions are the largest sources of atmospheric ethane in the preindustrial atmosphere

Supporting Information:
- Text S1, Figures S1–S4, and Tables S1–S6

Correspondence to:
M. R. Nicewonger,
nicewonm@uci.edu

Citation:
Nicewonger, M. R., K. R. Verhulst, M. Aydin, and E. S. Saltzman (2016), Preindustrial atmospheric ethane levels inferred from polar ice cores: A constraint on the geologic sources of atmospheric ethane and methane, *Geophys. Res. Lett., 43*, 214–221, doi:10.1002/2015GL066854.

Received 2 NOV 2015
Accepted 7 DEC 2015
Accepted article online 12 DEC 2015
Published online 6 JAN 2016

Preindustrial atmospheric ethane levels inferred from polar ice cores: A constraint on the geologic sources of atmospheric ethane and methane

Melinda R. Nicewonger[1], Kristal R. Verhulst[1,2], Murat Aydin[1], and Eric S. Saltzman[1]

[1]Department of Earth System Science, University of California, Irvine, California, USA, [2]Now at Jet Propulsion Laboratory, California Institute of Technology, Pasadena, California, USA

Abstract Ethane levels were measured in air extracted from Greenland and Antarctic ice cores ranging in age from 994 to 1918 Common Era (C.E.) There is good temporal overlap between the two data sets from 1600 to 1750 C.E. with ethane levels stable at 397 ± 28 parts per trillion (ppt) (±2 standard error (s.e.)) over Greenland and 103 ± 9 ppt over Antarctica. The observed north/south interpolar ratio of ethane (3.9 ± 0.1, 1σ) implies considerably more ethane emissions in the Northern Hemisphere than in the Southern Hemisphere, suggesting geologic ethane sources contribute significantly to the preindustrial ethane budget. Box model simulations based on these data constrain the global geologic emissions of ethane to 2.2–3.5 Tg yr^{-1} and biomass burning emissions to 1.2–2.5 Tg yr^{-1} during the preindustrial era. The results suggest biomass burning emissions likely increased since the preindustrial period. Biomass burning and geologic outgassing are also sources of atmospheric methane. The results place constraints on preindustrial methane emissions from these sources.

1. Introduction

Ethane (C_2H_6) is the most abundant nonmethane hydrocarbon in the atmosphere and is an important atmospheric pollutant. It is removed from the atmosphere via oxidation with the hydroxyl radical (OH) yielding a global average lifetime of roughly 2 months [*Xiao et al.*, 2008]. The major sources of atmospheric ethane today are the production, processing, transmission and use of oil and natural gas, and burning of biofuels, with total global emissions estimated at 11–15 Tg yr^{-1} [*Rudolph*, 1995; *Xiao et al.*, 2008; *Etiope and Ciccioli*, 2009; *Simpson et al.*, 2012]. The largest natural sources are biomass burning and geologic emissions. Minor emissions from oceanic and terrestrial ecosystems also occur [*Plass-Dülmer et al.*, 1995; *Clarkson et al.*, 1997; *Stein and Rudolph*, 2007]. Ethane sources also emit methane (CH_4), an important atmospheric pollutant and one of the largest contributors to global warming [*Hartmann et al.*, 2013]. As a result, atmospheric ethane variability can be used to constrain methane emissions from nonbiogenic sources [*Aydin et al.*, 2011; *Simpson et al.*, 2012].

At present, ethane emissions are predominantly located in the Northern Hemisphere due to fossil fuel production and use [*Rudolph*, 1995; *Xiao et al.*, 2008]. During 2000–2010 Common Era (C.E.), the mean annual ethane level was 1300–1400 parts per trillion (ppt) over Greenland and 200–250 ppt over Antarctica [*Simpson et al.*, 2006; *Aydin et al.*, 2011; *Blake*, 2013]. The large north/south (N/S) interpolar ratio of ethane (approximately 6:1) is due to the asymmetrical geographic distribution of ethane sources combined with the relatively short atmospheric lifetime. Measurements in polar firn air from both hemispheres indicate large increases in atmospheric ethane during the first half of the 20th century due to rising anthropogenic emissions, followed by a decline from 1980 to 2000 C.E. [*Aydin et al.*, 2011; *Worton et al.*, 2012]. Atmospheric ethane levels have been stable in the beginning of the 21st century [*Simpson et al.*, 2012; *Helmig et al.*, 2014].

This study presents the first atmospheric record of ethane based on measurements of air bubbles trapped in ice cores from Greenland and Antarctica. The Greenland samples are from a dry-drilled shallow ice core from Summit (Greenland Ice Sheet Project (GISP)2B ice core) and cover the time period from 1456 to 1862 C.E. The Antarctic samples are from West Antarctic Ice Sheet Divide (WAIS Divide, WDC-05A ice core) and cover the time period 994 to 1918 C.E. (see supporting information for site characteristics and chronologies). The implications for ethane emissions in the preindustrial atmosphere are examined using a steady state six-box photochemical model. The implications for preindustrial methane emissions are also examined.

2. Measurement Methods and Data

Ice core air is extracted by melting 150–300 g ice core samples under vacuum in a 3″ ID glass extraction chamber [*Verhulst*, 2014]. Prior to extraction, the outer 1–2 mm of the sample is scraped with a scalpel to eliminate surface contaminants. The sample is then placed inside the extraction chamber with a glass-sealed magnetic stir bar. Both the chamber and the sample are precooled to −40°C. The chamber is sealed using a flat ground glass flange with a 1/16″ OD indium wire. The indium wire O-ring is cleaned in 5% H_2SO_4 solution prior to use. The extraction chamber is immersed in a cold bath (dry ice/ethanol, −40°C) throughout the experiment except during melting. The chamber is connected to a glass vacuum line via glass valves fitted with PTFE O-ring seals (Glass Expansion, Australia) and a ½″ PTFE Swagelok fitting. The glass vacuum line is equipped with Glass Expansion valves and an oil-free pumping system (see supporting information).

Once the sample is loaded and a leak tight seal is achieved, the extraction chamber is flushed several times with clean N_2 to remove residual lab air, evacuated to ~5 mTorr, and isolated from the vacuum line to start the melting cycle (see supporting information). The cold bath is replaced with hot water (60°C) for 1 min, followed by warm water (30°C) for the remainder of the melting process. The hot water induces a thermal shock, fracturing the ice, and reducing melt time. The meltwater is magnetically stirred to further reduce the melt time (~30min) and to prevent excessive warming of the meltwater. At the end of the melt cycle, the warm bath is replaced by an ice bath (1–2°C), and the extracted air is cryogenically transferred into a stainless steel sample tube immersed in liquid helium (−269°C). The extracted air first passes through a cold trap (glass beads at −40°C) that removes excess water vapor but does not trap ethane. After 2 min of cryogenic pumping, the sample tube is isolated and allowed to warm to room temperature for analysis.

The ethane analysis is conducted using gas chromatography and high-resolution mass spectrometry with isotope dilution, which has been described in detail previously [*Aydin et al*., 2007, 2011; *Verhulst*, 2014]. A known amount of ^{13}C-ethane is added to each sample during the preconcentration stage. The abundance of ethane in the sample is calculated from the measured ^{13}C-ethane/^{12}C-ethane ratio. The calibration of the internal standard is based on high-pressure gas cylinders with known levels of ethane prepared in our laboratory from the pure compounds [*Aydin et al*., 2007]. The analytical uncertainty for ethane measured in a typical ice core sample (~20 cm^3 at STP) is ±3% (1σ).

Each sample analysis is followed by analysis of at least one N_2 blank to characterize the background (blank) ethane levels in the analytical extraction system. First, the sample meltwater is refrozen using the −40°C dry ice/ethanol bath while being pumped on to ensure full degassing. After several flushes with clean N_2, about 20 cm^3 at STP of clean N_2 is isolated above the refrozen ice core sample, and the melt/extraction process is repeated. We collected multiple blanks consecutively for most of the ice core samples (see supporting information). The consecutive blanks do not significantly differ from the first blank, suggesting the background ethane level is stable in the extraction system and ice core meltwater. For the blank correction, we subtract the moles of ethane in the average blank from the moles of ethane measured in a sample (see supporting information).

A total of 33 WDC-05A samples were analyzed for ethane. The WDC-05A measurements were conducted as three separate sets with 11 samples measured in 2011, 7 samples in 2012, and 15 samples in 2014 [*Verhulst*, 2014]. Ethane was analyzed in 27 GISP2B samples, with all measurements conducted in 2014. For both sites, the measurements were blank corrected using the average of all applicable blanks from the measurement year, excluding 2σ outliers. For the WDC-05A samples run in 2014, blanks were 0.09 ± 0.02 pmol (mean ± 1σ, $n = 12$), roughly 50% of the ethane measured in an average WDC-05A sample. The WDC-05A blanks from earlier years were higher and more variable (see supporting information). The blanks for the GISP2B samples were the same as WDC-05A blanks from 2014 and measured 0.09 ± 0.02 pmol (mean ± 1σ, $n = 27$), roughly 20% of the ethane in an average GISP2B sample. Blank variability is the largest source of measurement uncertainty. The overall uncertainty for an individual ice core measurement is calculated by propagating the variance in the calibrations and blanks and average ±7% and ±17% (1σ) for GISP2B and WDC-05A samples, respectively. Ethane is slightly more soluble in water at 0°C than air, leading to a small depletion of ethane in the air samples extracted with our wet-extraction method. We estimate the solubility-driven depletion of ethane to be less than 1% (see supporting information) and do not apply a correction to the measured ethane mixing ratios.

Several ice core samples (1 in WDC-05A; 9 in GISP2B) had measurable levels of chlorofluorocarbon (CFC-12 > 1 ppt). One WDC-05A sample and two GISP2B samples with the highest CFC-12 levels are not included in the

results (see supporting information). Additionally, one WDC-05A sample had elevated ethane levels (>500 ppt) due to a procedural error and is excluded from the results.

3. Results

The Greenland GISP2B samples cover the period from 1456 to 1862 C.E. at a resolution of 20–30 years (Figure 1a). Ethane levels from 1450 to 1750 C.E. range from 356 to 520 ppt with a mean of 409 ± 49 ppt (±1σ, $n = 17$). The mean annual ethane level over Greenland today is about 3 times higher at ~1300 ppt [*Aydin et al*., 2011; *Blake*, 2013; *Helmig et al*., 2014]. There is slightly more ethane in younger samples, with the measurements from 1750 to 1862 C.E. averaging 528 ± 37 ppt ($n = 8$). During the mid-1700s, atmospheric methane levels began increasing primarily due to the emergence of new anthropogenic sources (fossil fuels and biofuels and increased biomass burning) which also emit ethane [*Etheridge et al*., 1998; *MacFarling Meure et al*., 2006]. The increase in ethane levels in the GISP2B samples after 1750 C.E. may be the beginning of the increasing ethane trend in the Northern Hemisphere. However, the fact that many of the shallow GISP2B samples also have low but measurable levels of CFC-12 (1 ppt ≤ CFC-12 ≤ 10 ppt, Figure 1a) warrants some caution. The ethane rise in the Northern Hemisphere during the 1700s requires verification with measurements in CFC-free ice core air.

The WDC-05A samples from Antarctica cover the time period from 994 to 1918 C.E. but at lower resolution and with some gaps (Figure 1c). The ethane measurements from 1450 to 1750 C.E. range from 77 to 143 ppt with a mean of 106 ± 19 ppt ($n = 11$). There is twice as much ethane in the atmosphere over Antarctica today, with mean levels of 215 ppt from 2000 to 2010 C.E. [*Aydin et al*., 2011; *Blake*, 2013; *Helmig et al*., 2014]. Over the 900 year measurement period, ethane is highest around 1000 C.E. at nearly 200 ppt and steadily declines over the next few hundred years. A linear regression of the ethane data from 994 to 1336 C.E. indicates a decreasing trend (p value = 0.08). The WDC-05A measurements after 1750 C.E. are slightly higher at 131 ± 35 ppt ($n = 9$) but only because of three elevated replicates from 1918 C.E. (>150 ppt). The mean of the two sets of replicates from 1845 C.E. and 1884 C.E. is 112 ppt ($n = 5$) and is not significantly different from the 1450–1750 C.E. mean. Overall, 8 out of 10 replicate measurements from WDC-05A agree within analytical uncertainties. The two exceptions are samples older than 1400 C.E. and were analyzed in 2011 and 2012 when the blank uncertainties were larger (Table S1 in the supporting information).

Trace gases can be produced in situ within ice cores, for example, due to high impurity levels [*Saito et al*., 2007; *Faïn et al*., 2014], which result in elevated measurements that do not reflect the true atmospheric levels. Ideally, multiple ice core records from sites with different physical and chemical characteristics (e.g., temperature, accumulation rate, dust, and organic impurity levels) are needed to validate that the observed record is in fact an atmospheric signal. However, all other ice core ethane measurements we conducted so far are based on a dry-extraction method, which yields highly elevated levels with respect to the wet-extraction-based measurements shown here [*Aydin et al*., 2007] (also, see supporting information).

A less ideal way to validate the ice core trace gas measurements is to compare measurements in shallow ice cores with atmospheric records derived from firn air measurements. However, ice core and firn air measurements at the same site do not yield contemporaneous records because firn air sampling requires significant open porosity and permeability, while ice core measurements require closed porosity. Additionally, ice core samples within a few meters of the close-off depth can be contaminated by postcoring entrapment of modern air [*Aydin et al*., 2010].

In Greenland, our youngest GISP2B samples are about 100 years older than the oldest time period constrained by Summit firn air measurements (Figures 1a and 1b). Ethane measured in the shallowest GISP2B samples is considerably lower than the deepest firn air measurement. Similarly, ethane in the shallowest WDC-05A sample from Antarctica is lower than the deepest firn air measurements at WAIS Divide. There are no obvious inconsistencies between the firn air and ice core measurements from the same sites, and both the Greenland and Antarctic records are consistent with ethane levels rising during the 1800s and early 1900s from a lower preindustrial baseline.

Ethane measured in South Pole firn air constrains atmospheric ethane levels since about 1910 C.E. [*Aydin et al*., 2011]. The South Pole firn air record also shows a steep increase in ethane during the early 20th century (Figure 1c). However, three WDC-05A measurements from 1918 C.E. average 174 ± 14 ppt, while the South Pole firn air atmospheric history indicates ethane levels below 100 ppt at that time (Figure 1c). When

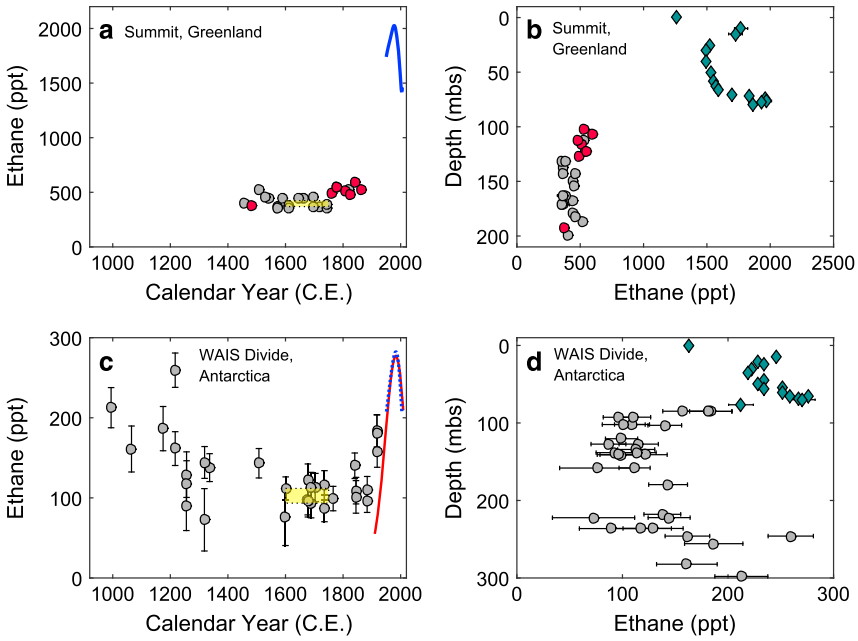

Figure 1. (a) GISP2B ice core ethane mixing ratios (gray and red circles) and the ethane atmospheric history from Summit derived from firn air measurements [*Aydin et al.*, 2011] (blue line). Samples with CFC-12 levels > 1 ppt are shown by the red circles. Also, see Figure S4 (supporting information). (b) Ethane measurements in firn air from Summit [*Aydin et al.*, 2011] (green diamonds) and ice core measurements from Figure 1a. (c) WDC-05A ice core ethane mixing ratios (gray circles) and WAIS Divide (blue dotted line) and South Pole (solid red line) ethane atmospheric histories derived from firn air measurements. (d) Ethane measurements in firn air from WAIS Divide (green diamonds) [*Aydin et al.*, 2011] and ice core measurements from Figure 1c. The yellow boxes in Figures 1a and 1c indicate the ethane mean ±2*s.e. during 1600–1750 C.E. used in the preindustrial simulations in Figure 2. Errors for the ice core and firn air measurements are ±1σ and ±2*s.e., respectively.

comparing ice core and firn air measurements from different sites, the relative accuracy of the dating techniques, as well as the different smoothing functions at the sites, has to be taken into account. For example, the older (deeper) air at the South Pole firn is more heavily smoothed (50–60 years width at half height) than the WAIS Divide ice core air (20 years width at half height). It is possible that small decadal scale fluctuations in atmospheric ethane could be recorded in WAIS Divide but not in South Pole. For a full assessment of how the WAIS Divide ice core record compares with the South Pole firn air measurements, more ice core measurements that overlap in time with the South Pole firn air record are needed.

4. Implications for the Preindustrial and Modern Ethane Budgets

The ice core ethane measurements and previous firn air measurements indicate a substantial increase in ethane during the 20th century due to human activities [*Aydin et al.*, 2011; *Worton et al.*, 2012]. The large interpolar ethane ratio in the modern atmosphere is mainly due to the emissions linked to fossil fuel production and use. Using zonally averaged surface flask measurements from 60–90°N and 60–90°S, we calculate the N/S Hemisphere interpolar ethane ratio to be 6.3 ± 0.1 (1σ) [*Aydin et al.*, 2011; *Blake*, 2013; *Helmig et al.*, 2014]. Natural geologic seeps also contribute to the N/S Hemispheric asymmetry due to the greater areal extent of near surface hydrocarbon deposits in the Northern Hemisphere (Table 1) [*Etiope and Ciccioli*, 2009]. By contrast, biomass burning emissions are located primarily in the tropics and are distributed more evenly between the hemispheres (Table 1) [*Duncan et al.*, 2003; *Xiao et al.*, 2008].

The Greenland and Antarctic ice core measurements from 1600 to 1750 C.E. allow an estimate of the preindustrial ethane interpolar ratio. The mean ethane levels for this time period are 397 ± 28 ppt (±2 standard error (s.e.)) over Greenland and 103 ± 9 ppt (±2 s.e.) over Antarctica, yielding an interpolar ratio of 3.9 ± 0.1 (±1σ). Clearly, ethane emissions in the Northern Hemisphere were considerably larger than those in the Southern Hemisphere even in the absence of fossil fuel emissions. It is evident from these observations that natural ethane emissions from geologic seeps contributed significantly to the preindustrial ethane budget.

Table 1. Global Ethane Emissions Inferred Using a Six-box Atmospheric Model

Source (Tg C_2H_6 yr^{-1})	NH/total[a]	Preindustrial 1600–1750 C.E.	Modern Era 1980 C.E.	Modern Era 2000–2010 C.E.
Fossil fuel	0.93	0	11.3–14.8	5.9–8.4
Geologic	0.85	2.2–3.5	2.2–3.5	2.2–3.5
Total fossil[b]		2.2–3.5	14.5–17.4[b]	9.0–11.0[b]
Biofuel	0.80	0.50	1.5	2.0
Biomass burning	0.58	1.2–2.5	2.1–4.3	1.7–3.3
Total non-fossil		1.7–3.0	3.6–5.8	3.7–5.3

[a]The spatial distribution assumed for each source is given as the Northern Hemispheric fraction and is described further in the supporting information.
[b]The calculation of the total fossil term requires the summation of the fossil fuel and geologic sources, which are dependent terms in the box model solutions. A low fossil fuel source cannot be added to a low geologic source. Rather, a low fossil source requires a geologic source near the high end of the geologic range.

We use a steady state model to quantify changes in the global ethane budget implied by the ice core ethane data from 1600 to 1750 C.E. The model consists of six zonal tropospheric boxes (three in each hemisphere), representing 30° wide latitude bands [*Marik*, 1998; *Mitchell et al*., 2013]. Ethane exchange between adjacent boxes occurs via transport parameters calibrated to the observed distribution of SF_6. The oxidation of ethane in the model is based on the climatological OH, pressure, and temperatures from *Spivakovsky et al*. [2000] and the temperature dependent reaction rate constant from *Sander et al*. [2006]. This yields a global average ethane lifetime of 90 days via reaction with OH. The latitudinal distribution of ethane sources is based on literature estimates (Table 1 and supporting information). Fossil fuel emissions are assumed zero. Biofuel emissions are small and prescribed according to *van Aardenne et al*. [2001] (Table 1).

In the simulations, geologic and biomass burning sources are allowed to vary independently from 1–5 Tg yr^{-1} at 0.01 Tg yr^{-1} increments. Ethane mixing ratios in the polar latitudes (60–90°) are calculated for all permutations of geologic and biomass burning emissions. The results are compared to the ice core data, and scenarios are considered viable when the calculated ethane mixing ratios in the 60–90°N and 60–90°S boxes are within ±2 s.e. of the preindustrial mean from the ice core observations (1600–1750 C.E., yellow box in Figures 1a and 1c). In the viable scenarios, geologic emissions range from 2.2 to 3.5 Tg yr^{-1} and biomass burning from 1.2 to 2.5 Tg yr^{-1} (Figure 2). Note that biomass burning and geologic source strengths cannot vary independently within these ranges. When biomass burning emissions are low, geologic emissions are high, and vice versa, with a sum always greater than 4.4 Tg yr^{-1}. The model results show that while both geologic and biomass burning emissions contribute significantly to the preindustrial ethane budget, geologic emissions are the largest natural source. Our estimate of 2.2–3.5 Tg yr^{-1} of geologic ethane emissions during 1600–1750 C.E. is in close agreement with a present-day estimate of 2–4 Tg yr^{-1} [*Etiope and Ciccioli*, 2009].

The same six-box model is used to explore how our estimates of preindustrial geologic emissions impact our understanding of the modern ethane budget. Model simulations for the modern atmosphere are carried out for two time periods: (1) the peak in 20th century ethane (circa 1980 C.E.) when ethane in the high northern and southern latitudes peaked at about 2000 ppt and 280 ppt, respectively and (2) 2000–2010 C.E. when ethane in the high northern and southern latitudes were lower at approximately 1350 ppt and 215 ppt, respectively [*Simpson et al*., 2006; *Aydin et al*., 2011; *Blake*, 2013; *Helmig et al*., 2014]. Two separate simulations are carried out for each of these periods, with geologic emissions fixed at the low (2.2 Tg yr^{-1}) and high (3.5 Tg yr^{-1}) ends of the estimates from the preindustrial simulation. The ethane lifetime and the latitudinal distribution of sources are identical to the preindustrial simulations. Fossil fuel and biomass burning emissions are varied from 0 to 20 Tg yr^{-1} at 0.05 Tg increments. For the 1980 C.E. simulations, model results are considered viable (Figure 2a) when they are consistent with the firn air-based atmospheric history of ethane [*Aydin et al*., 2011], with ethane levels in the 60–90°N and 60–90°S boxes between 1900–2100 ppt and 265–295 ppt, respectively. For 2000–2010 C.E. simulations, model results are considered viable when they are consistent with flask air network measurements [*Simpson et al*., 2006; *Blake*, 2013; *Helmig et al*., 2014] with ethane levels for 60–90°N, 30°N–30°S, and 60–90°S in the ranges of 1285–1415 ppt, 475–525 ppt, and 205–225 ppt, respectively (Figure 2a; see supporting information).

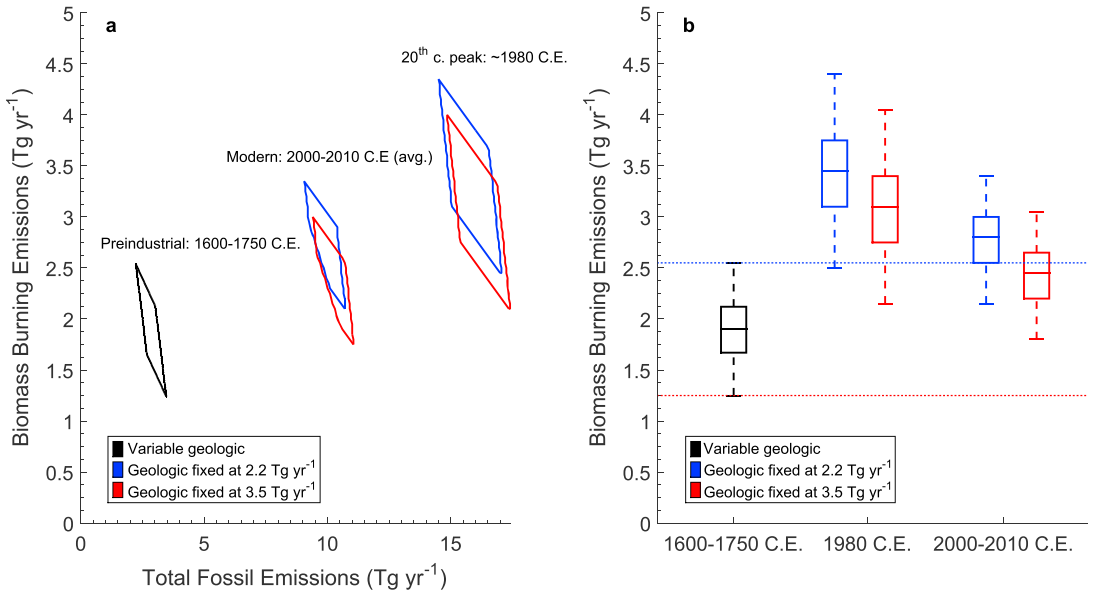

Figure 2. Six-box model results: (a) Preindustrial simulation for 1600–1750 C.E. (black contour) and modern atmosphere simulations for 1980 C.E. and 2000–2010 C.E. with geologic emissions constant at 2.2 Tg yr^{-1} (blue contour) and 3.5 Tg yr^{-1} (red contour). All permutations of total fossil (geologic only for preindustrial) and biomass burning emissions that fall within the enclosed contours yield viable solutions. (b) Box and whisker plots showing biomass burning emission estimates for the preindustrial and modern atmosphere simulations shown in Figure 2a. On each box, the center line is the median value, the edges of the box are the 25th and 75th percentiles, and the whiskers delineate the minimum and maximum of the data. The preindustrial box (black) depicts the range of biomass burning emissions for geologic emissions varying from 2.2 Tg yr^{-1} (blue dashed line) to 3.5 Tg yr^{-1} (red dashed line). The 1980 C.E. and 2000–2010 C.E. boxes depict the range of biomass burning emissions for geologic emissions fixed at 2.2 Tg yr^{-1} (blue) and 3.5 Tg yr^{-1} (red) for varying anthropogenic fossil fuel emissions.

These simulations yield ethane emissions that are consistent with prior published estimates for this period (Table 1) [*Xiao et al*., 2008; *Aydin et al*., 2011; *Simpson et al*., 2012] and indicate anthropogenic fossil fuel emissions of ethane decreased by roughly 45–50% from 11.3–14.8 Tg yr^{-1} to 5.9–8.4 Tg yr^{-1} from 1980 to 2000–2010 C.E. (Figure 2a). This is a slightly larger percent decrease than the prior estimate by *Aydin et al*. [2011]. The difference is due to the inclusion of constant geologic ethane emissions in the current analysis.

The model results also suggest ethane emissions from biomass burning likely increased since the preindustrial period. As noted before, biomass burning (1.2–2.5 Tg yr^{-1}) and geologic emissions (2.2–3.5 Tg yr^{-1}) cannot vary independently within the reported ranges but are inversely related. For the low-end geologic simulation for 1980 C.E. (blue box, Figure 2b), there are only a small number of solutions that suggest biomass burning emissions could have been constant since the preindustrial period near 2.5 Tg yr^{-1} (blue-dashed line, Figure 2b). For the 1980 C.E. case with high-end geologic emissions (red box, Figure 2b), all viable model simulations require higher biomass burning emissions than the preindustrial period (red-dashed line, Figure 2b). In the simulations for the 2000–2010 C.E. period, there are more solutions that allow biomass burning emissions to not be different than the preindustrial rates, but again, only if the geologic source strength is near the low-end estimate (2.2 Tg yr^{-1}, blue box, Figure 2b). If the geologic source strength is closer to the high-end estimate (3.5 Tg yr^{-1}, red-dashed line, Figure 2b), then the model results imply biomass burning emissions during the 2000–2010 C.E. period must have been greater than during the preindustrial period. Notably, none of the simulations estimate modern biomass burning emissions lower than preindustrial rates.

Methane and ethane are both emitted from biomass burning and natural geologic seeps. The ethane model results therefore provide constraints for preindustrial methane emissions. The methane:ethane emission ratio from biomass burning is 7–8 (Tg per Tg) [*Andreae and Merlet*, 2001]. An emission ratio of 7.5 implies methane emissions from biomass burning in the 9–19 Tg yr^{-1} range during 1600–1750 C.E., which is consistent with prior estimates of 14–17 Tg yr^{-1} based on methane stable isotope measurements ($\delta^{13}CH_4$) in Antarctic ice cores [*Ferretti et al*., 2005; *Mischler et al*., 2009]. The methane:ethane emission ratio from geologic sources is highly variable [*Jones et al*., 1999]. *Etiope and Ciccioli* [2009] used gas composition measurements from petroleum seepage areas and soil-gas data worldwide to estimate globally averaged geologic emissions of ethane (2–4 Tg yr^{-1}) and methane (42–64 Tg yr^{-1}), yielding a globally averaged methane:ethane emission

ratio of 16–21 (Tg per Tg). Our estimate of geologic ethane emission falls within the range estimated by *Etiope and Ciccioli* [2009], suggesting their geologic methane emissions estimate of 42–64 Tg yr^{-1} is likely accurate. Our results suggest the methane:ethane emission ratio from geologic sources is closer to 17–19 (Tg per Tg) on a global average basis.

5. Conclusions

This study presents the first preindustrial atmospheric ethane record based on ice core measurements. The measurements strongly suggest that a paleoatmospheric ethane signal is preserved in the ice core air bubble archive. The principle challenge in inferring atmospheric ethane levels from ice core measurements is minimizing and quantifying analytical blanks associated with the gas extraction and analysis. Future work will focus on reducing the uncertainties and verifying and extending this ice core record with additional measurements using Greenland and Antarctic ice cores.

This study highlights the importance of geologic emissions in the natural budgets of ethane and methane. The persistent N/S asymmetry of preindustrial ethane implies that a combination of emissions from biomass burning and natural geologic seeps is required, with geologic emissions being the larger of the two. The underlying assumption is that the geographic distribution of ethane sources did not change over time (i.e., geographic source distributions in our box model are constant). Large temporal changes in the latitudinal distribution of biomass burning or geologic emissions during the study period would alter the inferred strengths of these sources.

Little is known about the temporal variability in the strength of geologic emissions. It may be reasonable to assume that hydrocarbon emissions from geologic seeps remain relatively constant over centennial time scales. However, during glacial/interglacial transitions, it is possible that geologic emissions fluctuate in response to the variable crustal loading caused by changes in ice sheets and sea level (e.g., via faulting during isostatic rebound) as well as due to changes in the exposure of continental shelves [*Etiope*, 2012; *Walter Anthony et al*., 2012]. Longer ice core ethane records will allow investigation of long-term variability in geologic hydrocarbon emissions into the atmosphere.

This study also demonstrates the potential for using ethane to constrain the magnitude of biomass burning emissions in the preindustrial atmosphere. We infer from the ice core ethane records that biomass burning emissions likely increased since the preindustrial period. The WAIS Divide ethane record indicates ethane levels were relatively high around 1000 C.E., steadily declined until 1600 C.E., plateaued for several hundred years, and then rose sharply around 1900 C.E. This temporal trend is similar to the variability in the biomass burning record inferred from ice core CH_4 and CO [*Ferretti et al*., 2005; *Wang et al*., 2010] but requires verification with measurements from different ice cores. An extended ice core ethane record from both poles will help constrain variability in biomass burning emissions over longer time scales, providing insight into climatic influences on biomass burning.

Acknowledgments
This research was supported by the National Science Foundation grants PLR-1204248 and PLR-1043780. M.R.N. was supported by an NSF Graduate Research Fellowship (DGE-1321846). K.R.V. was supported by the UC Irvine Faculty Mentor Program Fellowship during a portion of this work. E.S.S. received support from the NSF Independent Research and Development program. Data supporting the analysis and conclusion can be found in the supporting information.

References

Andreae, M. O., and P. Merlet (2001), Emission of trace gases and aerosols from biomass burning, *Global Biogeochem. Cycles*, *15*(4), 955–966, doi:10.1029/2000GB001382.

Aydin, M., M. B. Williams, and E. S. Saltzman (2007), Feasibility of reconstructing paleoatmospheric records of selected alkanes, methyl halides, and sulfur gases from Greenland ice cores, *J. Geophys. Res.*, *112*, D07312, doi:10.1029/2006JD008027.

Aydin, M., et al. (2010), Post-coring entrapment of modern air in some shallow ice cores collected near the firn-ice transition: Evidence from CFC-12 measurements in Antarctic firn air and ice cores, *Atmos. Chem. Phys.*, *10*(11), 5135–5144, doi:10.5194/acp-10-5135-2010.

Aydin, M., K. R. Verhulst, E. S. Saltzman, M. O. Battle, S. A. Montzka, D. R. Blake, Q. Tang, and M. J. Prather (2011), Recent decreases in fossil-fuel emissions of ethane and methane derived from firn air, *Nature*, *476*, 198–201, doi:10.1038/nature10352.

Blake, D. (2013), Methane, nonmethane hydrocarbons, alkyl nitrates, and chlorinated carbon compounds including 3 Chlorofluorocarbons (CFC-11, CFC-12, and CFC-113) in Whole-Air Samples, Carbon Dioxide Information Analysis Center, Oak Ridge Natl. Lab., U.S. Department of Energy, Oak Ridge, Tenn.

Clarkson, T. S., R. J. Martin, and J. Rudolph (1997), Ethane and propane in the Southern marine troposphere, *Atmos. Environ.*, *31*(22), 3763–3771, doi:10.1016/S1352-2310(97)00220-3.

Duncan, B. N., R. V. Martin, A. C. Staudt, R. Yevich, and J. A. Logan (2003), Interannual and seasonal variability of biomass burning emissions constrained by satellite observations, *J. Geophys. Res.*, *108*(D2), 4040, doi:10.1029/2002JD002378.

Etheridge, D. M., L. P. Steele, R. J. Francey, and R. L. Langenfelds (1998), Atmospheric methane between 1000 A.D. and present: Evidence of anthropogenic emissions and climatic variability, *J. Geophys. Res.*, *103*(D13), 15,979–15,993, doi:10.1029/98JD00923.

Etiope, G. (2012), Climate science: Methane uncovered, *Nat. Geosci.*, *5*, 373–374, doi:10.1038/ngeo1483.

Etiope, G., and P. Ciccioli (2009), Earth's degassing: A missing ethane and propane source, *Science*, *323*, 478, doi:10.1126/science.1165904.

Faïn, X., J. Chappellaz, R. H. Rhodes, C. Stowasser, T. Blunier, J. R. Mcconnell, E. J. Brook, and S. Preunkert (2014), High resolution measurements of carbon monoxide along a late Holocene Greenland ice core: Evidence for in situ production, *Clim. Past*, *10*, 987–1000, doi:10.5194/cp-10-987-2014.

Ferretti, D. F., et al. (2005), Unexpected changes to the global methane budget over the past 2000 years, *Science*, *309*, 1714–1717, doi:10.1126/science.1115193.

Hartmann, D. L., et al. (2013), Observations: Atmosphere and surface, in *Climate Change 2013: The Physical Science Basis. Contribution of Working Group I to the Fifth Assessment Report of the Intergovernmental Panel on Climate Change*, edited by T. F. Stocker et al., Cambridge Univ. Press, Cambridge, U. K., and New York.

Helmig, D., J. Hueber, and P. Tans (2014), Non-methane hydrocarbons from the NOAA ESRL surface network 2004-2013.

Jones, V. T., M. D. Matthews, and D. M. Richers (1999), Light hydrocarbons for petroleum and gas prospecting, in *Geochemical Remote Sensing of the Subsurface*, *Handbook of Explor. Geochem*., vol. 7, edited by G. J. S. Govett and M. Hale, Elsevier, New York.

MacFarling Meure, C., D. Etheridge, C. Trudinger, P. Steele, R. Langenfelds, T. Van Ommen, A. Smith, and J. Elkins (2006), Law Dome CO_2, CH_4 and N_2O ice core records extended to 2000 years BP, *Geophys. Res. Lett.*, *33*, L14810, doi:10.1029/2006GL026152.

Marik, T. (1998), Atmospheric $\delta^{13}C$ and δD measurements to balance the global methane budget, PhD thesis, Ruprecht-Karls-Univ., Heidelberg, Germany.

Mischler, J. A., T. A. Sowers, R. B. Alley, M. Battle, J. R. McConnell, L. Mitchell, T. Popp, E. Sofen, and M. K. Spencer (2009), Carbon and hydrogen isotopic composition of methane over the last 1000 years, *Global Biogeochem. Cycles*, *23*, GB4024, doi:10.1029/2009GB003460.

Mitchell, L., E. Brook, J. E. Lee, C. Buizert, and T. Sowers (2013), Constraints on the late Holocene anthropogenic contribution to the atmospheric methane budget, *Science*, *342*, 964–966, doi:10.1126/science.1238920.

Plass-Dülmer, C., R. Koppmann, M. Ratte, and J. Rudolph (1995), Light nonmethane hydrocarbons in seawater, *Global Biogeochem. Cycles*, *9*(1), 79–100, doi:10.1029/94GB02416.

Rudolph, J. (1995), The tropospheric distribution and budget of ethane, *J. Geophys. Res.*, *100*(D6), 11,369–11,381, doi:10.1029/95JD00693.

Saito, T., Y. Yokouchi, S. Aoki, T. Nakazawa, and Y. Fujii (2007), Ice-core record of methyl chloride over the last glacial–Holocene climate change, *Geophys. Res. Lett.*, *34*, L03801, doi:10.1029/2006GL028090.

Sander, S. P., et al. (2006), Chemical kinetics and photochemical data for use in atmospheric studies evaluation number 15. NASA Jet Propulsion Laboratory Publication 06-2, Pasadena, Calif. [Availabe at http://jpldataeval.jpl.nasa.gov/.]

Simpson, I. J., F. S. Rowland, S. Meinardi, and D. R. Blake (2006), Influence of biomass burning during recent fluctuations in the slow growth of global tropospheric methane, *Geophys. Res. Lett.*, *33*, L22208, doi:10.1029/2006GL027330.

Simpson, I. J., M. P. Sulbaek Andersen, S. Meinardi, L. Bruhwiler, N. J. Blake, D. Helmig, F. S. Rowland, and D. R. Blake (2012), Long-term decline of global atmospheric ethane concentrations and implications for methane, *Nature*, *488*(7412), 490–494, doi:10.1038/nature11342.

Spivakovsky, C. M., J. A. Logan, S. A. Montzka, Y. J. Balkanski, D. B. A. Jones, L. W. Horowitz, A. C. Fusco, M. J. Prather, S. C. Wofsy, and M. B. McElroy (2000), Three-dimensional climatological distribution of tropospheric OH: Update and evaluation, *J. Geophys. Res.*, *105*(D7), 8931–8980, doi:10.1029/1999JD901006.

Stein, O., and J. Rudolph (2007), Modeling and interpretation of stable carbon isotope ratios of ethane in global chemical transport models, *J. Geophys. Res.*, *112*, D14308, doi:10.1029/2006JD008062.

van Aardenne, J. A., F. J. Dentener, J. G. J. Olivier, C. G. M. K. Goldewijk, and J. Lelieveld (2001), A 1°x1° resolution data set of historical anthropogenic trace gas emissions for the period 1890–1990, *Global Biogeochem. Cycles*, *15*(4), 909–928, doi:10.1029/2000GB001265.

Verhulst, K. R. (2014), Atmospheric histories of ethane and carbon monoxide from polar firn air and ice cores, PhD thesis, Univ. of California Irvine, Calif.

Walter Anthony, K. M., P. Anthony, G. Grosse, and J. Chanton (2012), Geologic methane seeps along boundaries of Arctic permafrost thaw and melting glaciers, *Nat. Geosci.*, *5*, 419–426.

Wang, Z., J. Chappellaz, K. Park, and J. E. Mak (2010), Large variations in Southern Hemisphere biomass burning during the last 650 years, *Science*, *330*(6011), 1663–6, doi:10.1126/science.1197257.

Worton, D. R., et al. (2012), Evidence from firn air for recent decreases in non-methane hydrocarbons and a 20th century increase in nitrogen oxides in the Northern Hemisphere, *Atmos. Environ.*, *54*, 592–602, doi:10.1016/j.atmosenv.2012.02.084.

Xiao, Y., J. A. Logan, D. J. Jacob, R. C. Hudman, R. Yantosca, and D. R. Blake (2008), Global budget of ethane and regional constraints on U.S. sources, *J. Geophys. Res.*, *113*, D21306, doi:10.1029/2007JD009415.